Probability of U.S. regional tornado outbreaks and their links to the springtime ENSO phases and North Atlantic SST variability

Sang-Ki Lee[1,2], Andrew T. Wittenberg[3], David B. Enfield[1], Scott J. Weaver[4], Chunzai Wang[2] and Robert M. Atlas[2]

[1]Cooperative Institute for Marine and Atmospheric Studies, University of Miami, Miami, FL

[2]Atlantic Oceanographic and Meteorological Laboratory, NOAA, Miami, FL

[3]NOAA Geophysical Fluid Dynamics Laboratory, Princeton, NJ

[4]Climate Prediction Center, NOAA, College Park, MD

Submitted to Geophysical Research Letters

July 2015

Corresponding author address: Dr. Sang-Ki Lee, NOAA, Atlantic Oceanographic and Meteorological Laboratory, 4301 Rickenbacker Causeway, Miami, FL 33149, USA.

E-mail: Sang-Ki.Lee@noaa.gov.

Abstract

This study shows that the four main phases of springtime El Niño-Southern Oscillation (ENSO) evolution (persistent versus early-terminating El Niño, and resurgent versus transitioning La Niña) are linked to distinctive spatial patterns of the probability of U.S. regional tornado outbreaks. In particular, the outbreak probability increases significantly up to 27% over the Ohio Valley, Upper Midwest and Southeast when a La Niña persists into the spring and is followed by another La Niña (i.e., resurgent La Niña). The probability also increases significantly up to 38%, but mainly in the South, when a two-year La Niña transitions to an El Niño (i.e., transitioning La Niña). This study also shows that the North Atlantic sea surface temperature tripole is linked to the tornado outbreak probability over the Southeast and Upper Midwest in early spring, although this link may not be completely distinct from ENSO. These changes in outbreak probability are shown to be largely consistent with remotely forced regional changes in the large-scale tropospheric circulation, low-level wind shear, moisture transports and extratropical storm activity.

1. Introduction

The latest U.S. Natural Hazard Statistics reported that during 2004-2013 tornadoes claimed 1,091 lives in the U.S., only trailing behind heat-related fatalities, and caused 21.6 billion dollars in property and crop damages (Table S1). An early prognosis of tornadogenesis combined with an effective warning system will prevent many deaths and serious injuries. A parallel effort to expand the current severe weather outlooks beyond seven days will also help emergency managers, government officials, businesses and the public to better prepare their resources to save lives and to protect critical infrastructure.

As summarized in a recent review [*Tippet et al*., 2014], notable advances have been made since 2011, the year of the record-breaking tornado outbreaks in the U.S., on the potential of expanding the severe weather outlook at the National Oceanic and Atmospheric Administration (NOAA) beyond weather time scales [*Tippett et al.*, 2012; *Weaver et al*., 2012; *Barrett and Gensini*, 2013; *Lee et al*., 2013; *Thompson and Roundy*, 2013; *Elsner and Widen*, 2014; *Allan et al*., 2015]. Among others, *Lee et al*. [2013] showed that the majority of the extreme U.S. tornado outbreaks in the most intense tornado months of April and May during 1950-2010 were linked to a positive Trans-Niño (i.e., a positive zonal gradient of sea surface temperature anomalies (SSTAs) from the central tropical Pacific (CP) to the eastern tropical Pacific (EP)), typically occurring during the boreal spring following the peak of La Niña [*Trenberth and Stepaniak*, 2001; *Lee et al*., 2014a]. They showed using observations and modeling experiments that a positive Trans-Niño could enhance large-scale atmosphere conditions conducive to intense tornado outbreaks over the U.S. via extratropical teleconnections. Recently, *Allen et al*. [2015] showed that La Niña events persisting into the spring could increase U.S. tornado activity, especially over Oklahoma, Arkansas and northern Texas, and vice versa for El Niño events persisting into the spring. They used March-April-May (MAM) SSTAs in the Nino3.4 region (120°W-180°W and 5°S-5°N) to identify El Niño-Southern Oscillation (ENSO) events persisting into the spring. *Krishnamurthy et al*. [2015] further showed that the seasonal phasing of ENSO is critical to its impacts on the North American low-level jets, which influence U.S. tornado activity by controlling low-level vertical wind shear and moisture availability [*Muñoz and Enfield*, 2011; *Weaver et al.*, 2012].

These recent findings have identified ENSO as a potential source of seasonal predictability for U.S. tornado activity. However, it should be noted that ENSO usually decays rapidly in spring, which is the most active tornado season, shortly after reaching its peak in winter. During this time, the SSTAs in the tropical Pacific are typically much weaker in amplitude and their spatial structure becomes much less coherent [e.g., *Lee et al*. 2014a]. Additionally, every ENSO event is somewhat different from others, which is especially true during the springtime ENSO phase evolution [*Trenberth and Stepaniack*, 2001; *Chiang and Vimont*, 2004; *Yu and Kim*, 2010; *Lee et al*., 2014a; *Yeh et al*., 2014; *Capotondi et al.,* 2015]. For example, an ENSO event, while weakening during or after spring, may subsequently evolve into the onset of another ENSO event with either the same or opposite sign in the subsequent months (e.g., 1986-1987 El Niño, 1987-1988 El Niño and 1988-1989 La Niña). Hence, it is unlikely that the complexity of springtime ENSO phase evolution can be characterized by using a single ENSO index such as the Nino3.4 index or Trans-Niño index.

Given the previous finding that ENSO may provide the seasonal predictability of U.S. tornado outbreaks in spring, there is a clear need to better characterize the springtime ENSO phase evolution and its link to U.S. tornado activity. On this issue, a new method was recently presented to objectively characterize and explore the differences in the space-time evolution of equatorial Pacific SSTAs observed during El Niño events [*Lee et al*., 2014b]. An application of this method to the 21 El Niño events during 1949-2013 captured two leading orthogonal modes, which explain more than 60% of the inter-event variance. The first mode distinguishes a strong and persistent El Niño from a weak and early-terminating El Niño (Figures 1a and 1b). A similar analysis applied to the 22 La Niña events during 1949-2013 also revealed two leading orthogonal modes, with its first mode distinguishing a resurgent La Niña and a transitioning La Niña (Figures 1c and 1d).

The main objective of this study is to further advance our understanding of the relationship between the springtime ENSO phase evolution and regional U.S. tornado outbreaks. To achieve this and to move forward with the goal of developing a seasonal outlook for U.S. tornado outbreaks, we first present a new metric to measure the probability of tornado outbreaks within an area centered at a given geographic location (section 2). Then, we use that metric to explore the probability of tornado outbreaks in various regions of the U.S. under the four dominant phases of springtime ENSO evolution identified in *Lee et al*. [2014b] (section 3) and to explain the associated atmospheric processes (section 4). We also report a potential link between the North Atlantic SST tripole and U.S. regional tornado outbreaks in early spring (section 5). Finally, we discuss further research that is needed to develop a seasonal outlook (section 6).

2. Statistical Methods and Data Used

To develop a seasonal outlook for U.S. tornado outbreaks, it is important to understand exactly what a seasonal outlook can and cannot predict. First of all, tornadogenesis is a mesoscale problem that requires overlap of very specific and highly localized atmospheric conditions [e.g., *Doswell and Bosart*, 2001]. Therefore, it cannot be adequately captured by large-scale and long-term averaged atmospheric fields. In other words, a seasonal outlook cannot pinpoint exactly when, where and how many tornadoes may strike. Instead, a seasonal outlook may predict in terms of probability which regions are more vulnerable to, or more likely to experience, a widespread outbreak of tornadoes.

To move forward with the goal of developing a seasonal outlook, we propose a tornado outbreak index, which can be used to measure the probability that a tornado outbreak may occur in a predefined region. The following steps describe a method to compute the proposed tornado outbreak index for 1950 - 2014 using the Severe Weather Database (SWD) from NOAA. The Fujita scale-0 (F0) tornadoes are excluded in our analysis to avoid a spurious long-term trend in the SWD [e.g., *Verbout et al*., 2006; *Lee et al*., 2013]. Additionally, the number of F1-F5 tornadoes is weighted in such a way that one F*n* tornado is treated as *n* number of F1 tornadoes.

1) The first step is to count the weighted number of F1-F5 tornadoes within a circle of 200 km radius from the center of each 1°×1° grid point for 5 consecutive days. This is referred to as a 5-day overlapping tornado density - one value for each day and grid point.
2) The second step is to define the outbreak threshold as the 99th percentile of the tornado density values for each calendar month and grid point. Note that different threshold values are used for each grid point and calendar month to account for the regionally and seasonally inhomogeneous distribution of tornado statistics.
3) The final step is to identify months with one or more *outbreak days* to construct the monthly U.S. regional tornado outbreak index for each grid point.

For a subset of data, the numbers of outbreak and non-outbreak years can be counted to compute the probability of U.S. regional tornado outbreaks. Figure S1 shows the outbreak threshold values of the tornado density, and the 90th and 95th percentile probabilities of U.S.

regional tornado outbreaks for March, April and May, obtained by using the steps described above.

In the following sections, we explore the probability of tornado outbreaks in various regions of the U.S. under the four dominant phases of springtime ENSO evolution (Figure 1). We use the Extended Reconstructed Sea Surface Temperature version 3b (ERSST3), an in situ analysis of global monthly SST on a 2°×2° grid [*Smith et al*., 2008], to compute the leading modes of ENSO variability for the period of 1949-2013 as discussed in *Lee et al*. [2014b]. The Twentieth Century Reanalysis (20CR) [*Compo et al*., 2011] and the National Centers for Environmental Prediction-National Center for Atmospheric Research (NCEP-NCAR) reanalysis [*Kalnay et al*., 1996] are also used to derive atmospheric anomalies associated with the four dominant phases of springtime ENSO evolution.

3. Springtime ENSO Phases and Their Links to U.S. Regional Tornado Outbreaks

Figure 1 shows the time-longitude plots of the tropical Pacific SSTAs, averaged between 5°S and 5°N, for the four leading cases of ENSO variability reproduced from *Lee et al*. [2014b]. The first case exhibits strong and positive SSTAs in the EP during the peak season persisting throughout the boreal spring (+1), and thus is referred to as a strong and persistent El Niño case (e.g., 1982-1983 El Niño); hereafter, any month/season in an ENSO onset year is identified by the suffix (0), whereas any month/season in an ENSO decay year by the suffix (+1). The second case is characterized by relatively weak positive SSTAs in the CP during the peak season and a rapid development of cold SSTAs in the EP shortly after the peak season, and thus is referred to as a weak and early-terminating El Niño case (e.g., 1963-1964 El Niño). The third case describes a La Niña persisting into the spring (+1) and evolving to another La Niña, and thus is referred to as a resurgent La Niña case (e.g., 1998-1999 La Niña). This case is also frequently referred to as a two-year La Niña in the literature [e.g., *DiNezio and Deser*, 2014]. Finally, the fourth case describes a two-year La Niña transitioning to an El Niño, and thus is referred to as a transitioning La Niña case (e.g., 1971-1972 La Niña). Note that these four leading cases of ENSO variability mainly describe ENSO phase evolution in the spring (+1) following the peak of ENSO in boreal winter. For more details on the atmosphere-ocean dynamics linked to the leading modes of ENSO variability, the reader is referred to *Lee et al*. [2014b].

Figure 2 shows the composite SSTAs for the four dominant phases of springtime ENSO evolution in MAM (+1) and the corresponding probability of regional tornado outbreaks in April (+1). See Figures S3-S6 in the supporting information for the composite SSTAs and the probability of outbreaks in March (+1) and May (+1). The gray dots indicate that the SSTAs are statistically significant at 90% based on a Student's *t*-test. Similarly, the black dots mean that the probability of tornado outbreaks is statistically significant at 90% based on the exact binomial test of the null hypothesis, i.e., the springtime ENSO phases have no effect on the probability of tornado outbreaks. For each case, we used eight to eleven actual ENSO events for the composite analysis based on the sign and amplitude of the leading principal components of El Niño and La Niña variability (see Table S2 for the list of ENSO events used).

As shown in Figures 2a and 2e, the probability of U.S. regional tornado outbreaks in April (+1) is low overall (5% or less) when a strong El Niño persists into the spring (+1) after its peak (i.e., persistent El Niño). The probability of outbreaks may reach as high as 25% along the Mississippi river and over New York and central Florida. However, they are statistically insignificant at the 90% confidence level. The overall low probability of outbreaks shown in Figure 2e implies that the outbreak frequency is largely suppressed by a strong El Niño that persists throughout the boreal spring (+1), as suggested by *Allen et al*. [2015]. However, the statistical significance of the reduction cannot be established since the frequency distribution of the outbreak chance is highly skewed to the right.

Similar to the persistent El Niño case, when a weak El Niño terminates early and cold SSTAs develop over the EP in the spring (+1) (i.e., early-terminating El Niño), the probability of outbreaks is also low overall (5% or less) although it increases somewhat in limited regions over Missouri and northern Texas in April (+1) (Figures 2b and 2f), and over Iowa, Wisconsin and Illinois in May (+1) (Figure S4f).

When a La Niña persists into the spring (+1) and evolves to another La Niña (i.e., resurgent La Niña), the probability of outbreaks increases significantly up to 27% in April (+1) in wide regions in the Ohio Valley, Southeast, Upper Midwest and Great Plains (see Figure S2 for the U.S. climate regions as defined by the National Climate Data Center), particularly Nebraska, Illinois, Indiana, Kentucky, Tennessee, Mississippi, Alabama, Georgia, Virginia, North Carolina and Wisconsin (Figures 2c and 2g). It is interesting to note that the record-breaking 2011 tornado outbreaks occurred during a resurgent La Niña. Similarly, the super tornado outbreaks in 1974 occurred during a resurgent La Niña.

As shown in Figure 2d, when a two-year La Niña transitions to an El Niño (i.e., transitioning La Niña), the cold SSTAs in the CP are nearly dissipated away while the warm SSTAs in EP become strong and statistically significant in MAM (+1). In this case, the probability of tornado outbreaks increases strongly and significantly up to 38% in the South U.S., particularly over Kansas, eastern Colorado and Texas in April (+1) (Figure 2h), and over southern Texas in March (+1) (Figure S6f).

Two important questions arise among others as to why the probability of U.S. regional tornado outbreaks increases in the spring following the peak of La Niña, and why the regions affected during the resurgent La Niña case are quite different from the regions affected during the transitioning La Niña case. We attempt to address these questions in the next section.

4. Springtime Atmospheric Variability over the U.S. Linked to ENSO Phases

It is well known that La Niña causes the winter atmospheric jet stream to take an unusually wavy southeastward path into the U.S. from southwestern Canada, thus bringing colder and drier upper level air to the U.S. Hence, the winter storm activity over the U.S. tends to increase, causing more frequent wet conditions particularly over the Ohio Valley [e.g., *Ropelewski and Halpert*, 1986; *Eichler and Higgins*, 2006; *Mo*, 2010]. As shown in Figure 3a, in the spring (+1) of the resurgent La Niña case, an anomalous cyclone develops over the U.S. bringing colder and drier upper-level air to the U.S., and thus the extratropical storm activity increases, suggesting that the mechanism through which La Niña affects U.S. weather in winter months still prevails in the spring (+1) of the resurgent La Niña case [*Lee et al*., 2014a]. The anomalous cyclone and the associated increase in equivalent barotropic winds in turn enhance the low-level vertical wind shear (850 - 1000 hPa) east of the Rockies, and shift the moisture stream originating from the Gulf of Mexico more toward the east (Figure 3b), thus producing a set of favorable atmospheric environments for tornado outbreaks in the Southeast and Ohio Valley, consistent with Figure 2g.

In the spring (+1) of the transitioning La Niña case, on the other hand, the extratropical storm activity decreases slightly over the South and Southeast. Consistent with this feature, an anomalous anticyclone forms east of the Rockies inducing anomalous southerly winds over the South (Figure 3c). Therefore, the low-level vertical wind shear increases over the South and the moisture stream from the Gulf of Mexico is enhanced more toward the South (Figure 3d). These changes in the atmospheric environments are largely consistent with the increased probability of tornado outbreaks in the South (Figure 2h).

The large-scale atmospheric patterns in the spring (+1) following the peak of El Niño are largely opposite to those following the peak of La Niña [e.g., *Lee et al*., 2014a]. Thus, as shown in Figure S7, the atmospheric environments over the U.S. linked to the persistent and early-terminating El Niño cases are largely unfavorable for tornado outbreaks, in line with Figures 2e and 2f.

5. North Atlantic SST Tripole and U.S. Regional Tornado Outbreaks

As shown in Figure S8, there is a coherent and statistically significant pattern of springtime SSTAs in the North Atlantic linked to the extreme U.S. tornado outbreaks (see Tables S3 for the list of extreme U.S. tornado outbreak years used). This pattern is very similar to the North Atlantic SST tripole, which is the dominant mode of interannual SST variability in the Atlantic in boreal winter and spring and is known to be linked to multiple forcing mechanisms including the North Atlantic Oscillation, tropical Atlantic variability and extratropical teleconnections from the tropical Pacific [e.g., *Xie and Tanimoto*, 1998; *Okumura et al*., 2001; *Peng et al*., 2002; *Wu et al*., 2007; *Schneider and Fan*, 2012]. Hence, we further explore the potential link between the North Atlantic SST tripole and the probability of U.S. regional tornado outbreaks. First, we performed an empirical orthogonal function (EOF) analysis of the North Atlantic SSTAs in MAM to sort the past 66 years (i.e., 1949-2014) based on the amplitude of the North Atlantic SST tripole mode (i.e., the leading EOF mode). Then, we selected the top (i.e., positive) 10 cases and the bottom (i.e., negative) 10 cases from the sorted years to perform composite analysis (see Table S4 for the list of the positive and negative North Atlantic SST tripole years used).

As summarized in Figures 4 and S9, the North Atlantic SST tripole is indeed linked to the probability of U.S. regional tornado outbreaks in March and April. During its negative phase (i.e., cold in the tropical North Atlantic, warm in the subtropical North Atlantic and cold in the subpolar North Atlantic), a robust anomalous anticyclone straddles the subtropical North Atlantic extending westward over the U.S. In March, the increase in the equivalent barotropic winds along the poleward half of the anomalous anticyclone enhances the low-level vertical wind shear over the Upper Midwest and Ohio Valley (Figure 4b). It appears that the moisture transport increases somewhat along the gulf coast mainly toward the Southeast, which is likely due to the increased SSTAs in the Gulf of Mexico (Figure 4c). These changes in the low-level vertical wind shear and moisture transport are fairly consistent with the significantly increased probability of tornado outbreaks in the Southeast and Upper Midwest (Figure 4a). In April, the anomalous anticyclone over the U.S. retreats to the east enhancing the moisture supply and the low-level vertical wind shear along the South and Great Plains (Figures S9a-S9c). These relationships are almost exactly the opposite during the positive phase of the North Atlantic SST tripole (Figures 4d-4f and S9d-S9f).

Although the results summarized in Figures 4 and S9 are promising, it must be noted that a negative phase of the North Atlantic SST tripole forms more frequently in the early spring following the peak of La Niña (Table S3). Therefore, it is unclear whether the North Atlantic SST tripole adds much to the predictability of U.S. regional tornado outbreaks. Further studies using model experiments and advanced statistical methods are needed to better understand the impact of North Atlantic SST variability on the probability of U.S. regional tornado outbreaks.

6. Discussion

This study illustrates the links between the leading modes of springtime ENSO variability and the probability of U.S. regional tornado outbreaks. However, the leading modes of El Niño and La Niña variability represent only about 35% of the total variance [*Lee et al.*, 2014b]. Thus, it is important to take into account the second leading modes, which represent an additional approximately 28% of the total variance [*Lee et al*., 2014b]. The two leading modes of ENSO variability and the North Atlantic SST tripole mode could be used as predictors of the monthly U.S. regional tornado outbreak index, using a logistic regression analysis [*Cox*, 1958]. The regression coefficients obtained from the logistic regression analysis could be used to estimate the probability of U.S. regional tornado outbreaks given the amplitudes of the three predictors. Combining this statistical tool with a dynamic seasonal forecast model, which could be used to obtain the three predictors with 1-3 months lead time, it might be possible to build a seasonal outlook for U.S. regional tornado outbreaks. To this end, it is quite promising that high-resolution climate models are now beginning to demonstrate skill in simulating and predicting seasonal variations in some of the elements critical to U.S. tornado outbreak risk [e.g., *Krishnamurthy et al.,* 2015; *Yang et al.,* 2015; *Jia et al.,* 2015].

Acknowledgments

We would like to thank James Elsner and Jeff Trapp for helpful comments and suggestions on the statistical methods used in this study, and Ghassan Alaka and Hua Chen for their thoughtful comments and careful reviews. This work was supported by NOAA/CPO through its MAPP program NA12OAR4310083 and by the base funding of NOAA/AOML. SWD and ERSST3 were provided by NOAA SPC at http://www.spc.noaa.gov/wcm and NOAA NCDC at http://www.ncdc.noaa.gov, respectively. NCEP-NCAR reanalysis and 20CR were provided by NOAA/ESRL/PSD at http://www.esrl.noaa.gov/psd.

References

Allen, J. T., M. K. Tippett, and A. H. Sobel (2015), Influence of the El Nino/Southern Oscillation on tornado and hail frequency in the United States. *Nature Geosci*., *8*, 278–283, doi:10.1038/ngeo2385.

Barrett, B. S., and V. A. Gensini (2013), Variability of central United States April–May tornado day likelihood by phase of the Madden-Julian Oscillation. *Geophys. Res. Lett.*, *40*, 2790-2795.

Chiang J. C. H., and D. J. Vimont (2004), Analogous Pacific and Atlantic meridional modes of tropical atmosphere - ocean variability. *J. Clim.*, *17*, 4143–4158.

Compo, G. P., et al. (2011), The twentieth century reanalysis project, *Q. J. R. Meteorol. Soc.*, *137*, 1-28, doi:10.1002/qj.776.

Cox, D. R. (1958), The regression analysis of binary sequences (with discussion). *J. Roy. Stat. Soc.*, *B20*, 215–242.

Capotondi, A., et al. (2015), Understanding ENSO diversity, *Bull. Am. Meteorol. Soc.*, doi:10.1175/BAMS-D-13-00117.1.

DiNezio, P. N., and C. Deser (2014), Nonlinear controls on the persistence of La Niña, *J. Clim.*, *27*, 7335–7355, doi:10.1175/JCLI-D-14-00033.1.

Doswell, C. A., III, and L. F. Bosart (2001), Extratropical synopticscale processes and severe convection. *Severe Convective Storms, Meteor. Monogr.*, No. 50, Amer. Meteor. Soc. 27–69.

Eichler, T., and W. Higgins (2006), Climatology and ENSO-related variability of North American extratropical cyclone activity, *J. Clim*., *19*, 2076–2093.

Elsner, J. B., and H. M. Widen (2014), Predicting spring tornado activity in the central Great Plains by 1 March. *Mon. Weather Rev.*, *142*, 259-267.

Jia, L. et al., (2015), Improved seasonal prediction of temperature and precipitation over land in a high-resolution GFDL climate model. *J. Clim.*, *28*, 2044-2062, doi:10.1175/JCLI-D-14-00112.1.

Kalnay, E. et al. (1996), The NCEP/NCAR 40-year reanalysis project. *Bull. Amer. Meteor. Soc*., *77*, 437–471.

Krishnamurthy, L., G. Vecchi, R. Msadek, A. Wittenberg, T. Delworth, and F. Zeng, (2015), The seasonality of the Great Plains low-level jet and ENSO relationship. *J. Clim.*, *28*, 4525-4544, doi:10.1175/JCLI-D-14-00590.1.

Lee, S.-K., R. Atlas, D. B. Enfield, C. Wang and H. Liu (2013), Is there an optimal ENSO pattern that enhances large-scale atmospheric processes conducive to major tornado outbreaks in the U.S.? *J. Clim*., *26*, 1626-1642, doi:10.1175/JCLI-D-12-00128.1.

Lee, S.-K., P. N. DiNezio, E.-S. Chung, S.-W. Yeh, A. T. Wittenberg and C. Wang (2014b) Spring persistence, transition and resurgence of El Nino. *Geophys. Res. Lett*., *41*, 8578-8585, doi:10.1002/2014GL062484.

Lee, S.-K., B. E. Mapes, C. Wang, D. B. Enfield and S. J. Weaver (2014a), Springtime ENSO phase evolution and its relation to rainfall in the continental U.S. *Geophys. Res. Lett*., *41*, 1673-1680, doi:10.1002/2013GL059137.

Mo, K. C. (2010), Interdecadal modulation of the impact of ENSO on precipitation and temperature over the United States, *J. Clim*., *23*, 3639–3656.

Muñoz, E., and D. B. Enfield (2011), The boreal spring variability of the Intra-Americas low-level jet and its relation with precipitation and tornadoes in the eastern United States. *Clim. Dyn.*, *36*, 247–259, doi:10.1007/s00382-009-0688-3.

Okumura, Y., S. P. Xie, A. Numaguti, and Y. Tanimoto (2001), Tropical Atlantic air–sea interaction and its influence on the NAO. *Geophys. Res. Lett., 28*, 1507–1510.

Peng, S., W. A. Robinson and S. Li (2002), North Atlantic SST forcing of the NAO and relationships with intrinsic hemispheric variability, *Geophys. Res. Lett.*, *29*, doi:10.1029/2001GL014043, 2002.

Ropelewski, C. F., and M. S. Halpert (1986), North American precipitation and temperature patterns associated with the El Niño - Southern Oscillation (ENSO), *Mon. Weather Rev.*, *114*, 2352–2362.

Schneider, E. K. and M. Fan (2012), Observed decadal North Atlantic tripole SST variability. Part II: diagnosis of mechanisms. *J. Atmos. Sci.*, *69*, 51–64.

Smith, T. M., R. W. Reynolds, T. C. Peterson, and J. Lawrimore (2008), Improvements to NOAA's historical merged land-ocean surface temperature analysis (1880–2006), *J. Clim.*, *21*, 2283–2296.

Thompson, D. B., and P. E. Roundy (2013), The relationship between the Madden-Julian Oscillation and US violent tornado outbreaks in the spring. *Mon. Weather Rev.*, *141*, 2087-2095.

Tippett, M. K., A. H. Sobel, and S. J. Camargo (2012), Association of U.S. tornado occurrence with monthly environmental parameters. *Geophys. Res. Lett.*, *39*, L02801, doi:10.1029/2011GL050368.

Tippett, M. K., J. T. Allen, V. A. Gensini, and H. E. Brooks (2014), Climate and hazardous convective weather. *Curr. Clim. Change Rep.*, *1*, 60-73, doi:10.1007/s40641-015-0006-6.

Trenberth, K. E., and D. P. Stepaniak (2001), Indices of El Niño evolution. *J. Clim.*, *14*, 1697–1701.

Verbout, S. M., H. E. Brooks, L. M. Leslie, and D. M. Schultz (2006), Evolution of the U.S. tornado database: 1954–2003. *Wea. Forecasting*, *21*, 86–93.

Weaver, S. J., S. Baxter, and A. Kumar (2012), Climatic role of North American low-level jets on U.S. regional tornado activity. *J. Clim.*, *25*, 6666 - 6683.

Wu, L., F. He, Z. Liu, and C. Li (2007), Atmospheric teleconnections of tropical Atlantic variability: interhemispheric, tropical–extratropical, and cross-basin interactions. *J. Clim., 20*, 856–870, doi:http://dx.doi.org/10.1175/JCLI4019.1.

Xie, S.-P. and Y. Tanimoto (1998), A pan-Atlantic decadal climate oscillation. *Geophys. Res. Lett.*, *25*, 2185-2155, doi:10.1029/98GL01525.

Yang, X. et al. (2015), Seasonal predictability of extratropical storm tracks in GFDL's high-resolution climate prediction model. *J. Clim.*, *28*, 3592-3611, doi:10.1175/JCLI-D-14-00517.1.

Yeh, S.-W., J.-S. Kug, and S.-I. An (2014), Recent progress on two types of El Niño: Observations, dynamics, and future changes, Asia-Pac. *J. Atmos. Sci*., *50*, 69–81.

Yu, J.-Y., and S. T. Kim (2010), Three evolution patterns of Central-Pacific El Niño, *Geophys. Res. Lett*., *37*, L08706, doi:10.1029/2010GL042810.

Figure captions:

Figure 1. Time-longitude plots of the leading orthogonal modes of the tropical Pacific SSTAs averaged between 5°S and 5°N for 21 El Niño and 22 La Niña events during 1949-2013, reproduced from *Lee et al*. [2014b], namely (a) the persistent El Niño, (b) early-terminating El Niño, (c) resurgent La Niña and (d) transitioning La Niña. The unit is in °C.

Figure 2. Composite (a-d) SSTAs for the four dominant phases of springtime ENSO evolution in MAM (+1) and (e-h) the corresponding probability of U.S. regional tornado outbreaks in April (+1). The gray dots in panels a-d indicate that the SSTAs are statistically significant at 90% based on a student-*t* test. The black dots in panels e-h indicate that the probability of tornado outbreaks is statistically significant at 90% based on a binomial test. The unit is in °C for the SSTAs and in % for the probability of tornado outbreaks.

Figure 3. (upper row) Anomalous geopotential height at 500 hPa (color shades) and variance of 5day high-pass filtered meridional winds at 300 hPa (contours), and (lower row) anomalous moisture transport (vectors) and low-level vertical wind shear (850 - 1000 hPa; color shades) in MAM (+1) for (a,b) the resurgent La Niña and (c,d) transitioning La Niña cases. The units are in gpm for geopotential height, in $m^2 s^{-2}$ for variance of meridional winds, in kg $m^{-1} s^{-1}$ for moisture transport, and in m s^{-1} for vertical wind shear.

Figure 4. (top row) Probability of U.S. regional tornado, (middle row) composite SSTAs (color shades) and geopotential height anomalies at 500 hPa (contours), and (bottom row) low-level vertical wind shear anomalies (color shades) and moisture transport anomalies (vectors) in

March for (a-c) the negative and (d-f) positive North Atlantic SST tripole. The unit is in % for the probability of tornado outbreaks, in °C for the SSTAs, in gpm for geopotential height, in kg m^{-1} s^{-1} for moisture transport, and in m s^{-1} for vertical wind shear.

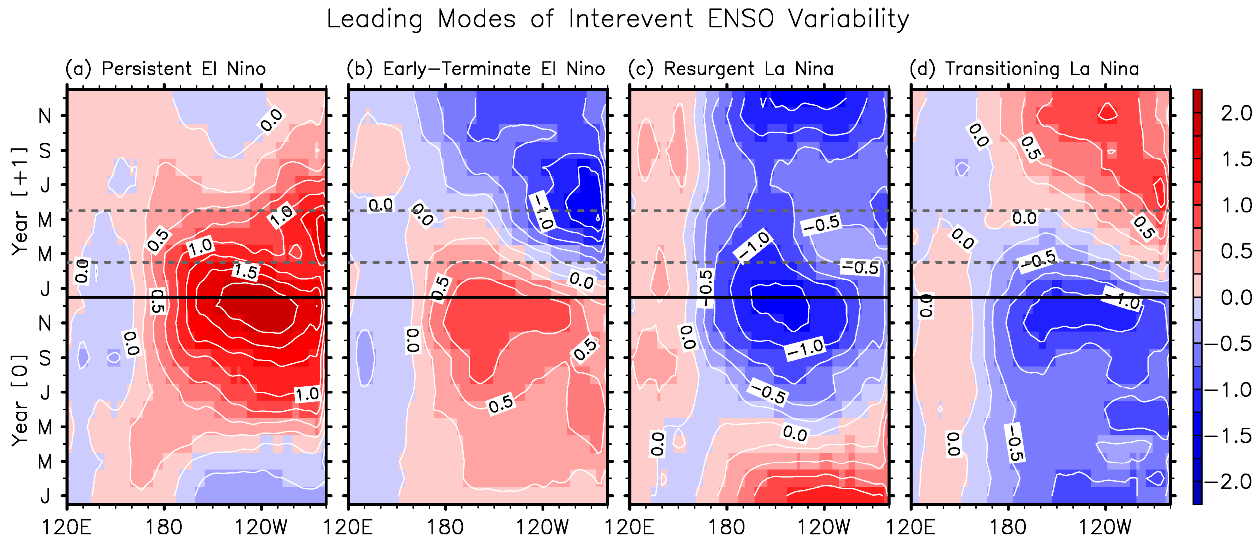

Figure 1. Time-longitude plots of the leading orthogonal modes of the tropical Pacific SSTAs averaged between 5°S and 5°N for 21 El Niño and 22 La Niña events during 1949-2013, reproduced from *Lee et al*. [2014b], namely (a) the persistent El Niño, (b) early-terminating El Niño, (c) resurgent La Niña and (d) transitioning La Niña. The unit is in °C.

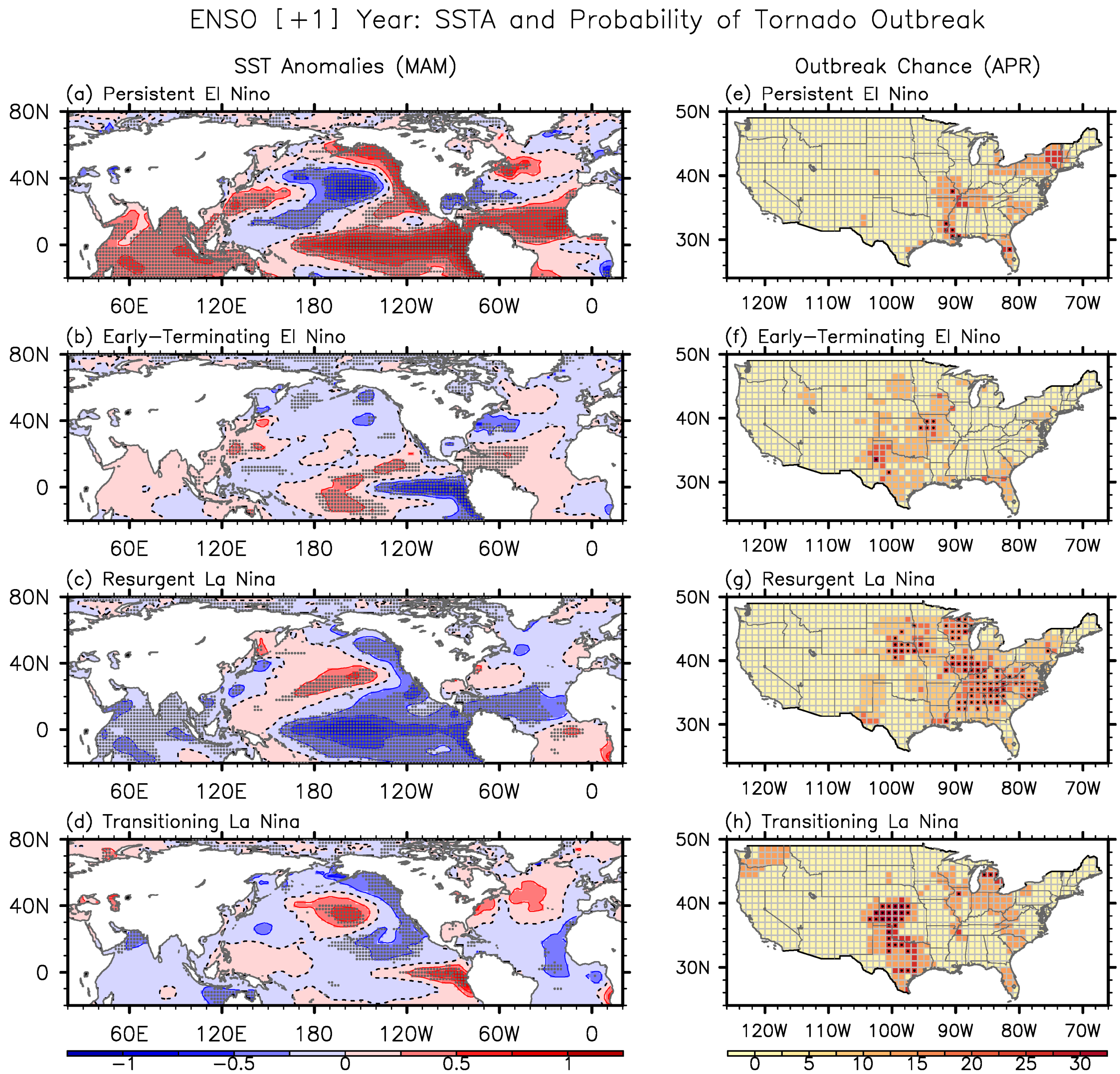

Figure 2. Composite (a-d) SSTAs for the four dominant phases of springtime ENSO evolution in MAM (+1) and (e-h) the corresponding probability of U.S. regional tornado outbreaks in April (+1). The gray dots in panels a-d indicate that the SSTAs are statistically significant at 90% based on a student-*t* test. The black dots in panels e-h indicate that the probability of tornado outbreaks is statistically significant at 90% based on a binomial test. The unit is in °C for the SSTAs and in % for the probability of tornado outbreaks.

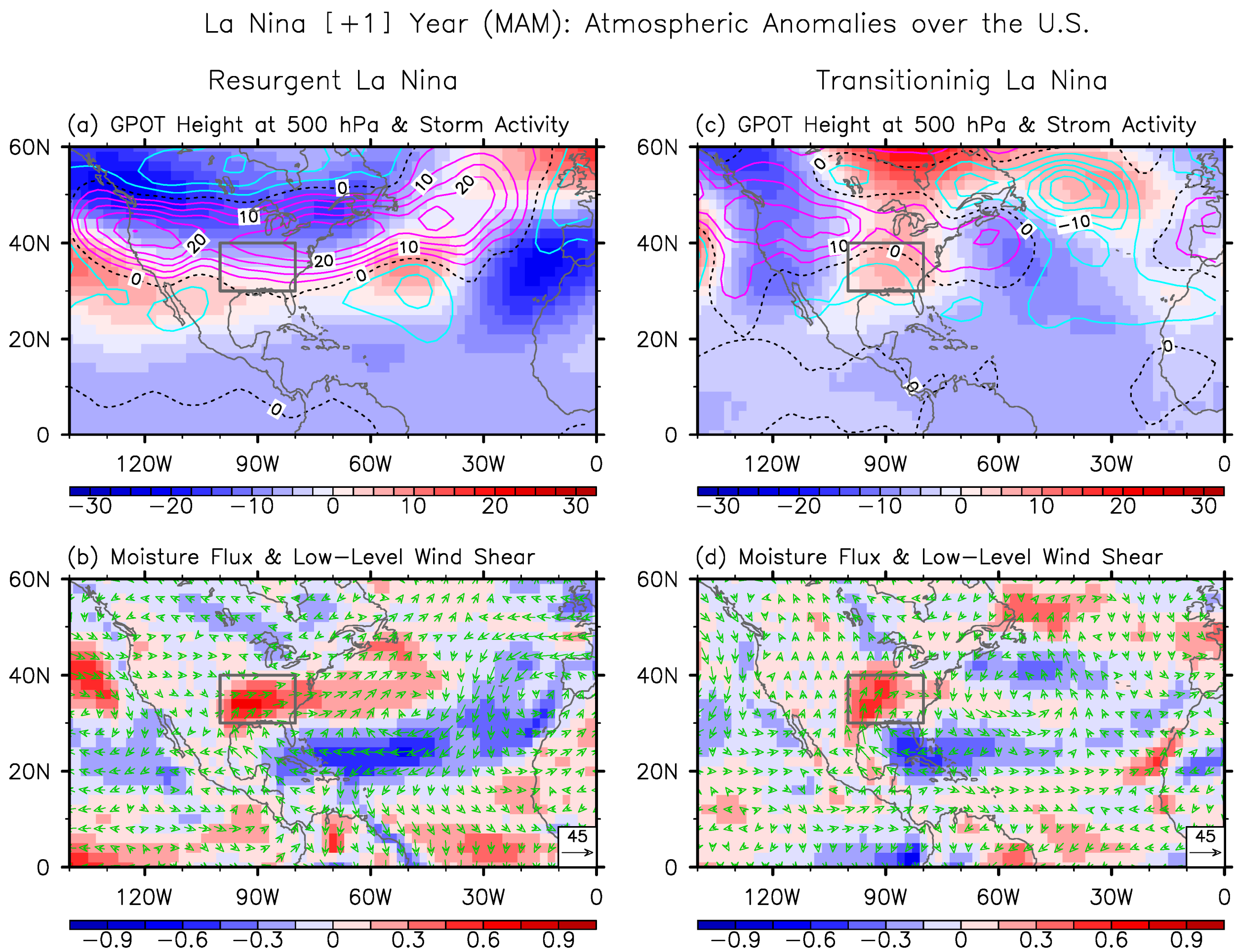

Figure 3. (upper row) Anomalous geopotential height at 500 hPa (color shades) and variance of 5day high-pass filtered meridional winds at 300 hPa (contours), and (lower row) anomalous moisture transport (vectors) and low-level vertical wind shear (850 - 1000 hPa; color shades) in MAM (+1) for (a,b) the resurgent La Niña and (c,d) transitioning La Niña cases. The units are in gpm for geopotential height, in $m^2 s^{-2}$ for variance of meridional winds, in $kg\ m^{-1} s^{-1}$ for moisture transport, and in $m\ s^{-1}$ for vertical wind shear.

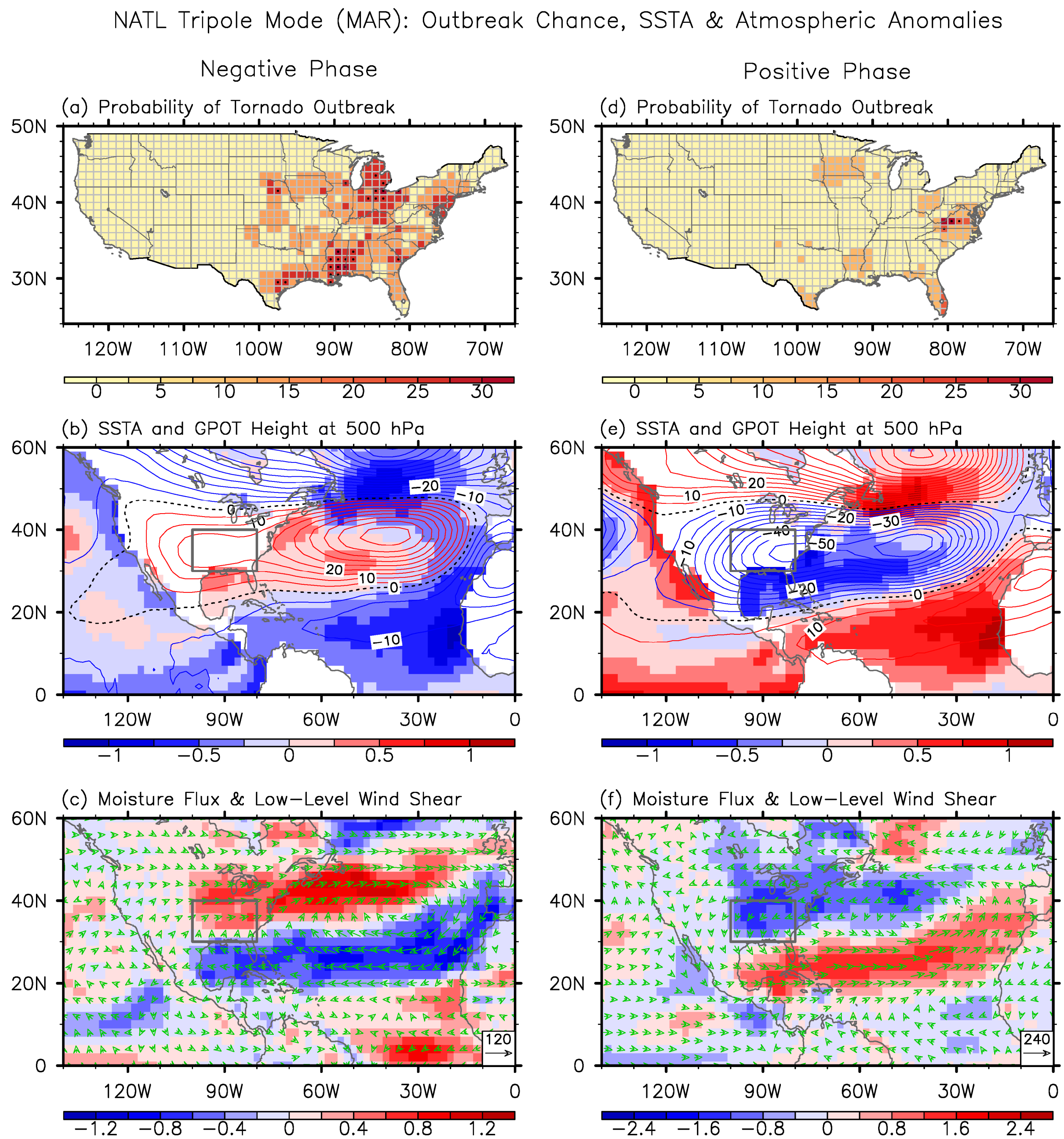

Figure 4. (top row) Probability of U.S. regional tornado, (middle row) composite SSTAs (color shades) and geopotential height anomalies at 500 hPa (contours), and (bottom row) low-level vertical wind shear anomalies (color shades) and moisture transport anomalies (vectors) in March for (a-c) the negative and (d-f) positive North Atlantic SST tripole. The unit is in % for

the probability of tornado outbreaks, in °C for the SSTAs, in gpm for geopotential height, in kg m^{-1} s^{-1} for moisture transport, and in m s^{-1} for vertical wind shear.

Table S1. Tornado-related number of fatalities and injuries and property and crop damages (in million US dollars) in the U.S. during 2004-2013, reproduced from the U.S. Natural Hazard Statistics (http://www.nws.noaa.gov/om/hazstats.shtml).

Year	Fatalities	Injuries	Property & crop damages
2004	35	396	549.2
2005	38	537	503.9
2006	64	990	759.0
2007	81	659	1,407.5
2008	**126**	**1,714**	**1,865.6**
2009	21	351	584.9
2010	45	699	1,134.6
2011	**553**	**5,483**	**9,493.0**
2012	70	822	1,649.7
2013	55	756	3,648.7
Total	**1,091**	**12,407**	**21,596.1**

Table S2. List of four leading cases of ENSO variability (i.e., 8 persistent El Niño, 10 early-terminating El Niño, 11 resurgent La Niña and 8 transitioning La Niña cases) identified based on the sign and amplitude of the principal components of interevent El Niño and La Niña variability during 1949 - 2013 [*Lee et al*., 2014b]. These ENSO events are listed by their onset-decay years (i.e., year (0) - year (+1)). Note that the four leading cases of ENSO variability describe ENSO phase evolution in the spring (+1) following the peak of ENSO in boreal winter.

Persistent El Niño	**Early-Terminating El Niño**	**Resurgent La Niña**	**Transitioning La Niña**
1957 - 1958	1951 - 1952	1949 - 1950	1950 - 1951
1968 - 1969	1953 - 1954	1955 - 1954	1956 - 1957
1982 - 1983	1963 - 1964	1970 - 1971	1964 - 1965
1986 - 1987	1965 - 1966	1973 - 1974	1971 - 1972
1991 - 1992	1969 - 1970	1974 - 1975	1975 - 1976
1997 - 1998	1972 - 1973	1983 - 1984	2000 - 2001
2004 - 2005	1977 - 1978	1984 - 1985	2005 - 2006
2009 - 2010	1987 - 1988	1988 - 1989	2011 - 2012
	1994 - 1995	1995 - 1996	
	2006 - 2007	1998 - 1999	
		2010 - 2011	

Table S3. List of 10 most active and 10 least active U.S. tornado years based on the total number of F1-F5 tornados in the U.S. during MAM. The corresponding ENSO phase for each case is also shown. Note that the decaying phase of 2008 La Niña cannot be described using the leading mode of observed La Niña variability; thus it is simply referred to as decaying La Niña. The onset of El Niño in 1982 occurred from ENSO neural condition; thus it is referred to as developing El Niño as in cases of 1991 and 2002.

10 Most Active U.S. Tornado Years		**10 Least Active U.S. Tornado Years**	
Year (Number)	**ENSO phases**	**Year (Number)**	**ENSO phases**
2011 (690)	Resurgent La Niña	1951 (67)	Transition La Niña
1973 (412)	Early-Term El Niño	1987 (80)	Persistent El Niño
1974 (390)	Resurgent La Niña	1950 (89)	Resurgent La Niña
2008 (359)	Decaying La Niña	2005 (89)	Persistent El Niño
1982 (342)	Developing El Niño	1952 (93)	Early-Term El Nino
1976 (325)	Transition La Niña	1992 (102)	Persistent El Niño
1957 (317)	Transition La Niña	1958 (113)	Persistent El Niño
2003 (306)	Persistent El Niño	2002 (125)	Developing El Niño
1991 (302)	Developing El Niño	1993 (129)	ENSO neutral
1965 (301)	Transition La Niña	1969 (130)	Persistent El Niño

Table S4. List of 10 negative and 10 positive phases of North Atlantic SST tripole mode in MAM during 1949-2014, derived from the leading EOF mode of the North Atlantic SSTAs in MAM. For each case of the positive and negative phase of North Atlantic SST tripole mode, the corresponding springtime ENSO phase is also listed. Note that the onset of El Niño in 1986 occurred from ENSO neural condition; thus it is referred to as developing El Niño as in cases of 1991, 1994 and 2009.

Negative phase of North Atlantic SST tripole (MAM)		**Positive phase of North Atlantic SST tripole (MAM)**	
Year	**ENSO phases**	**Year**	**ENSO phases**
1972	Transition La Niña	1951	Transition La Niña
1974	Resurgent La Niña	1958	Persistent El Niño
1975	Resurgent La Niña	1966	Early-Term El Nino
1976	Transition La Niña	1969	Persistent El Niño
1985	Resurgent La Niña	1970	Early-Term El Nino
1986	Developing El Niño	1981	ENSO neutral
1989	Resurgent La Niña	1983	Persistent El Niño
1991	Developing El Niño	1998	Persistent El Niño
1994	Developing El Niño	2005	Persistent El Niño
2009	Developing El Niño	2010	Persistent El Niño

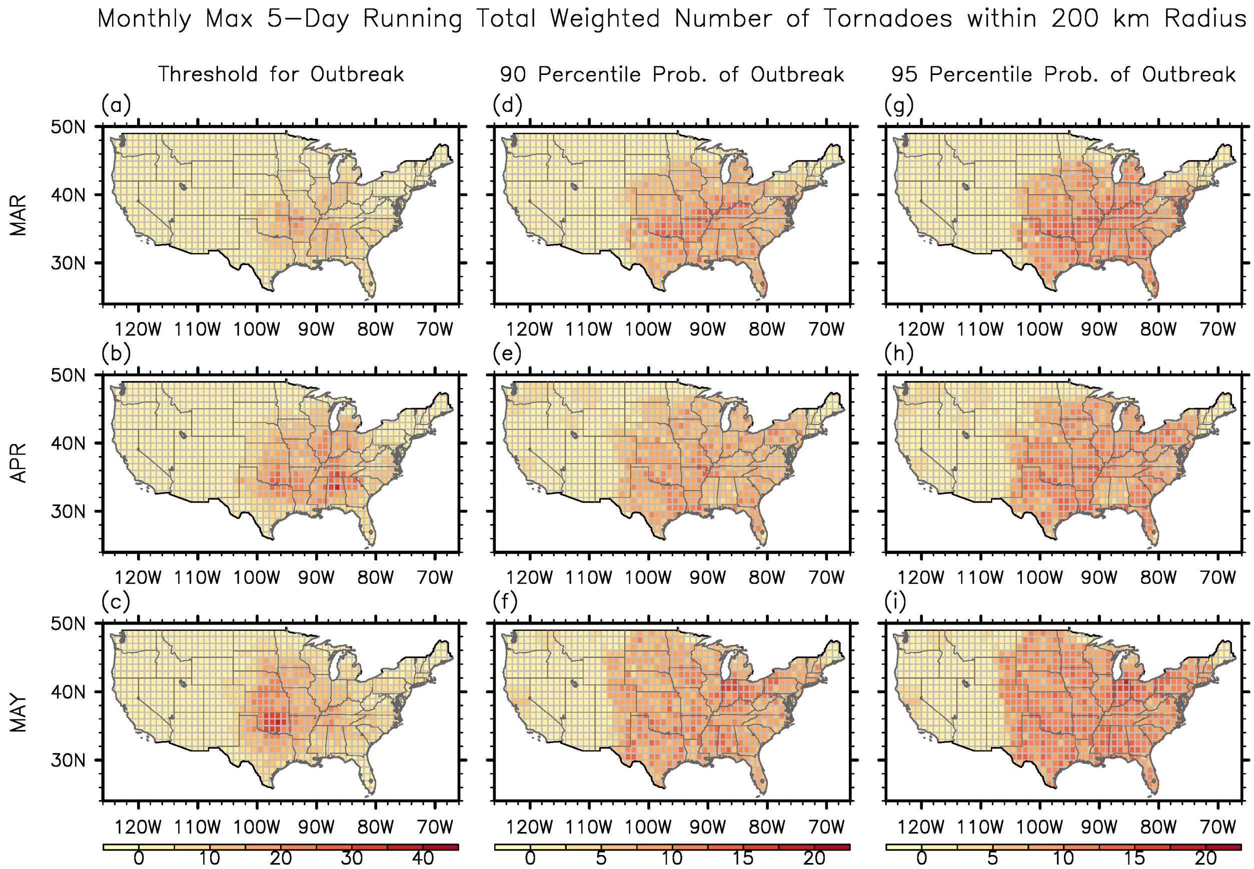

Figure S1. (a-c) Outbreak threshold of monthly maximum 5-day running total weighted number of F1 – F5 tornadoes within the 200 km radius, (d-f) the 90 percentile probability of U.S. regional outbreaks, and (g-i) the 95 percentile probability of U.S. regional tornado outbreaks for (top row) March, (middle row) April and (bottom row) May. Bootstrap method is used to determine the 90th and 95th percentile probabilities (%) of outbreak. See section 2 for more details about how these fields are derived.

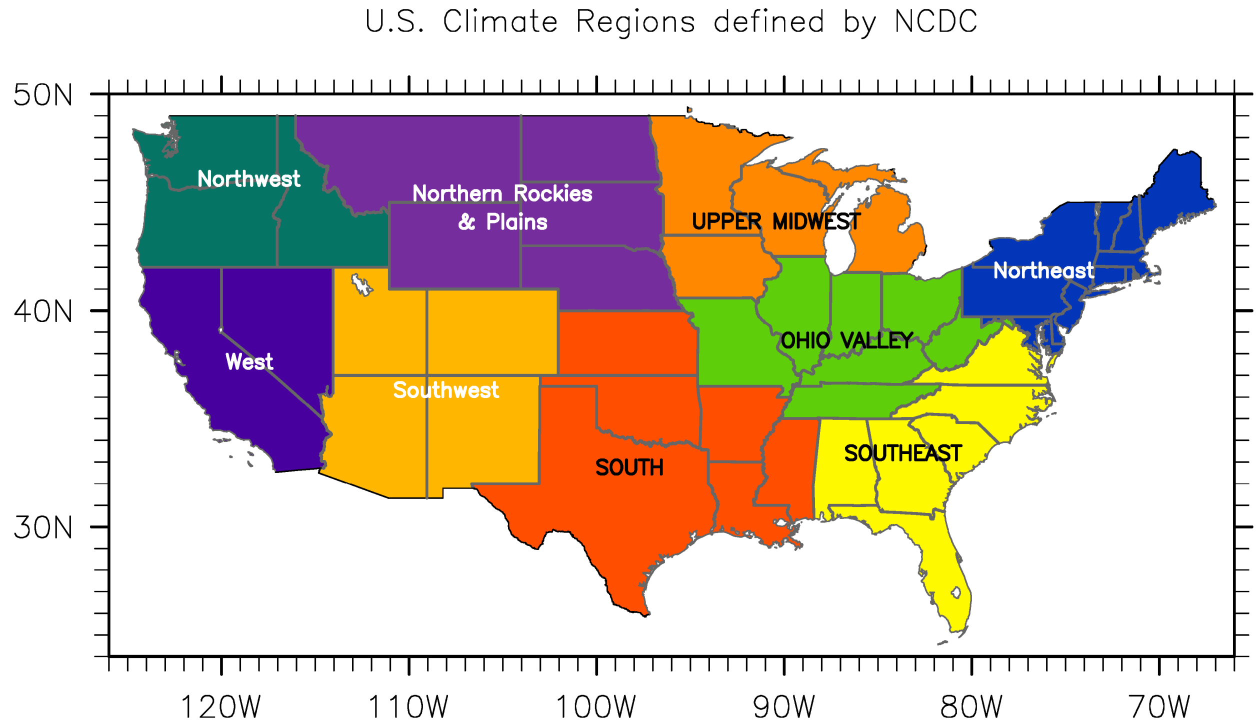

Figure S2. U.S. climate regions defined by National Climate Data Center. The four regions, namely the South, Ohio Valley, Southeast and Upper Midwest, are frequently referred in the main text to describe the probability of U.S. regional tornado outbreaks.

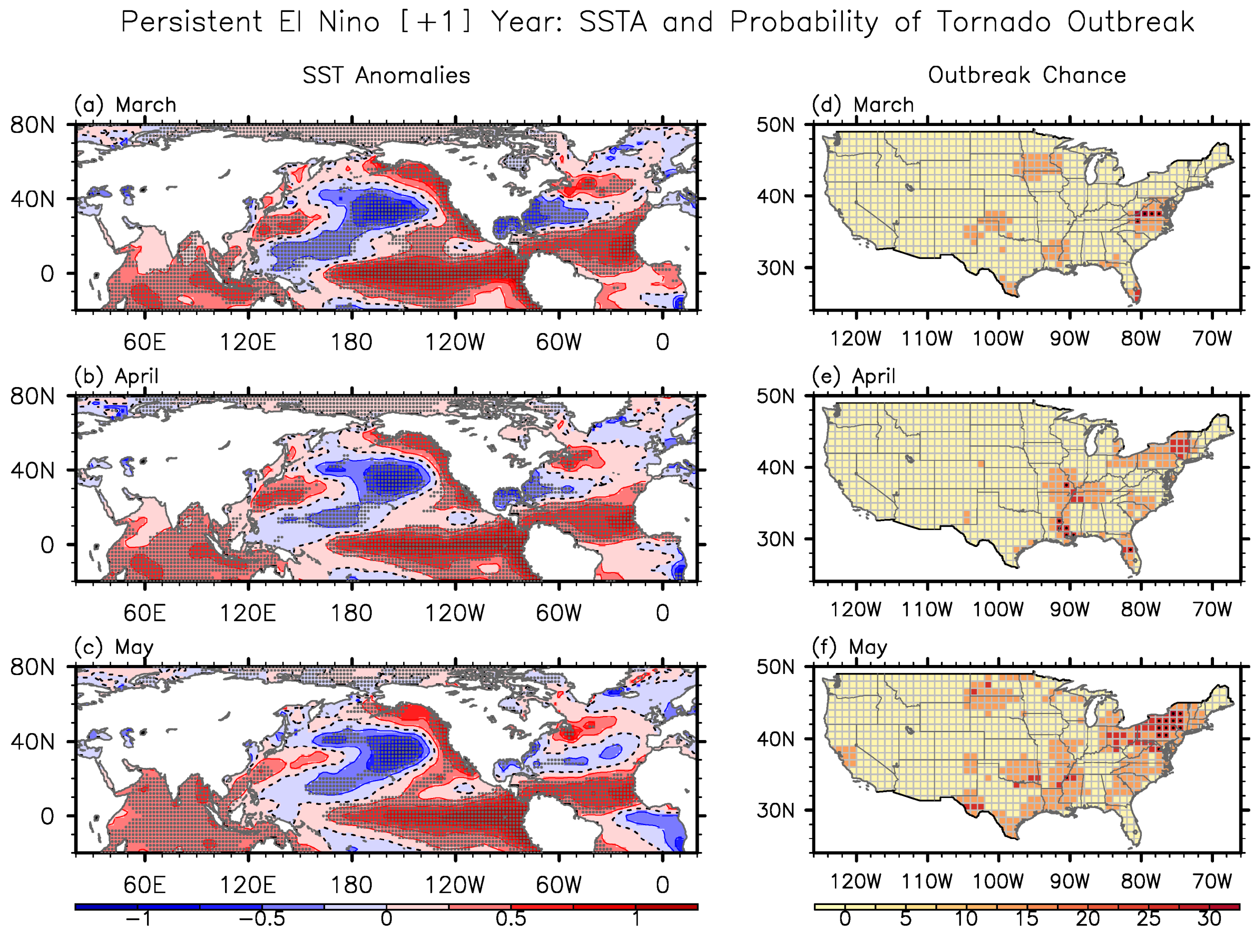

Figure S3. Composite (a-c) SSTAs for the persistent El Niño case and (d-f) the corresponding probability of U.S. regional tornado outbreaks in (top row) March (+1), (middle row) April (+1) and (bottom row) May (+1). The gray dots in panels a-c indicate that the SSTAs are statistically significant at 90% based on a Student's *t*-test. The black dots in panels d-f indicate that the probability of tornado outbreaks is statistically significant at 90% based on a binomial test. The unit is in °C for the SSTAs and in % for the probability of tornado outbreaks.

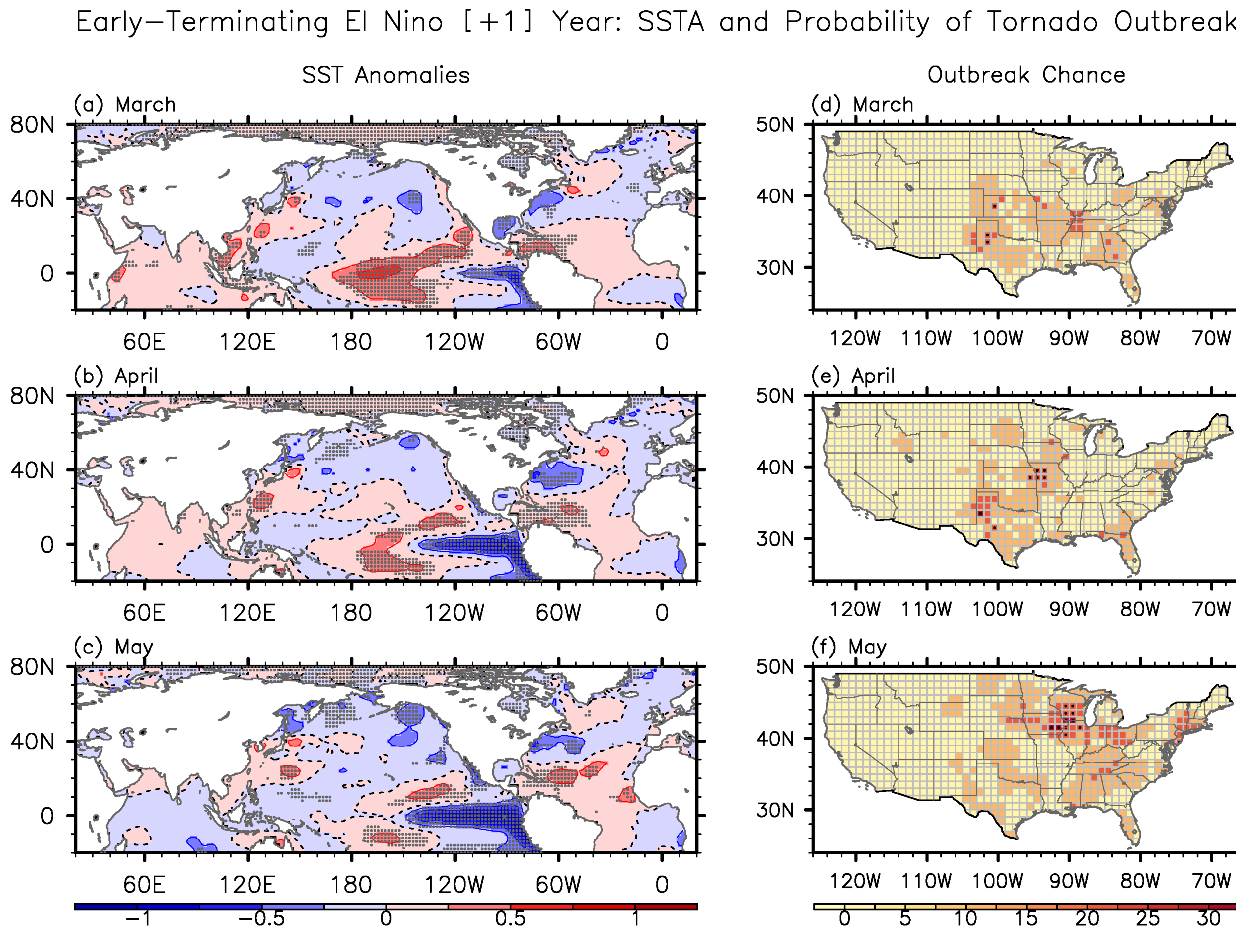

Figure S4. Composite (a-c) SSTAs for the early-terminating El Niño case and (d-f) the corresponding probability of U.S. regional tornado outbreaks in (top row) March (+1), (middle row) April (+1) and (bottom row) May (+1). The gray dots in panels a-c indicate that the SSTAs are statistically significant at 90% based on a Student's *t*-test. The black dots in panels d-f indicate that the probability of tornado outbreaks is statistically significant at 90% based on a binomial test. The unit is in °C for the SSTAs and in % for the probability of tornado outbreaks.

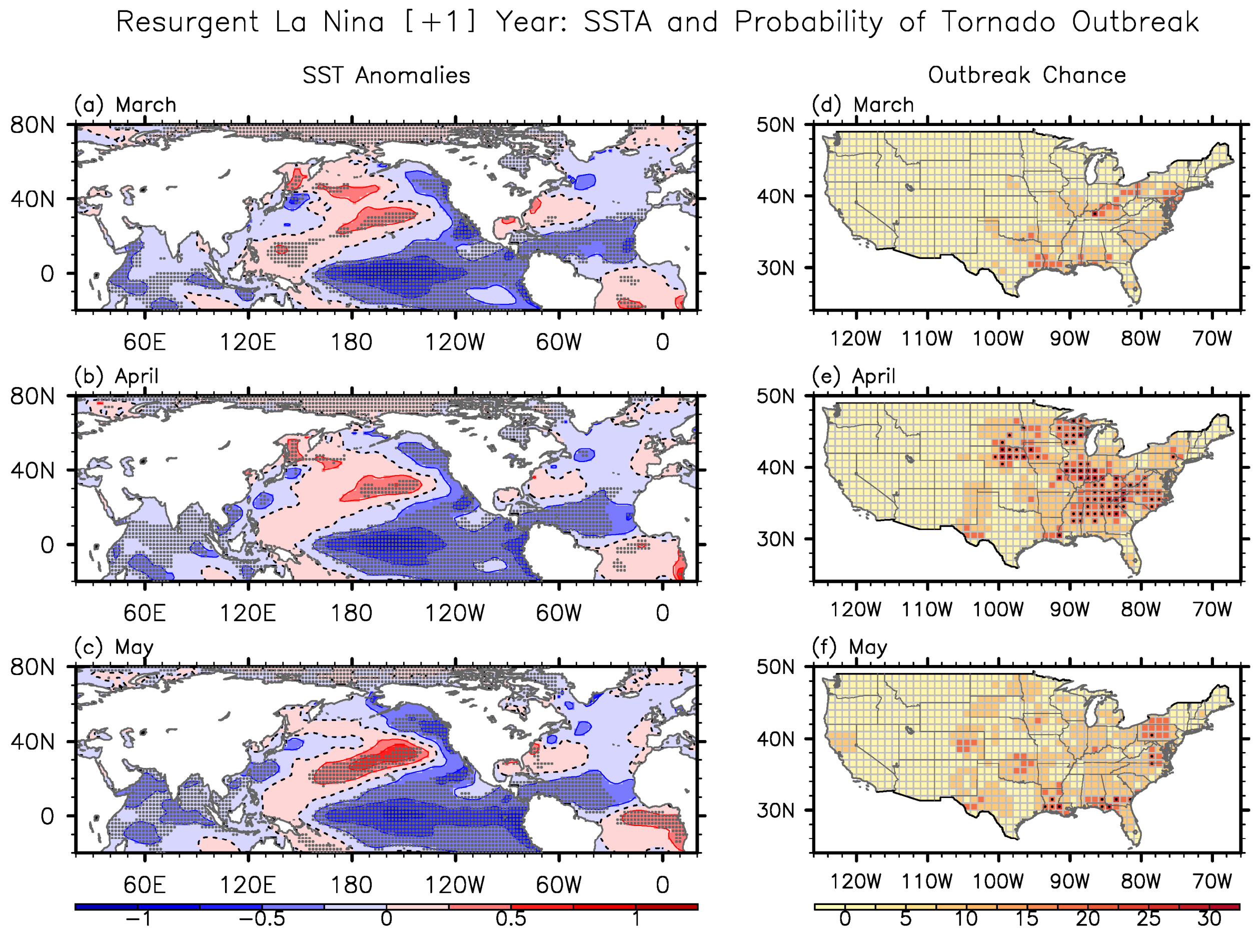

Figure S5. Composite (a-c) SSTAs for the resurgent La Niña case and (d-f) the corresponding probability of U.S. regional tornado outbreaks in (top row) March (+1), (middle row) April (+1) and (bottom row) May (+1). The gray dots in panels a-c indicate that the SSTAs are statistically significant at 90% based on a Student's *t*-test. The black dots in panels d-f indicate that the probability of tornado outbreaks is statistically significant at 90% based on a binomial test. The unit is in °C for the SSTAs and in % for the probability of tornado outbreaks.

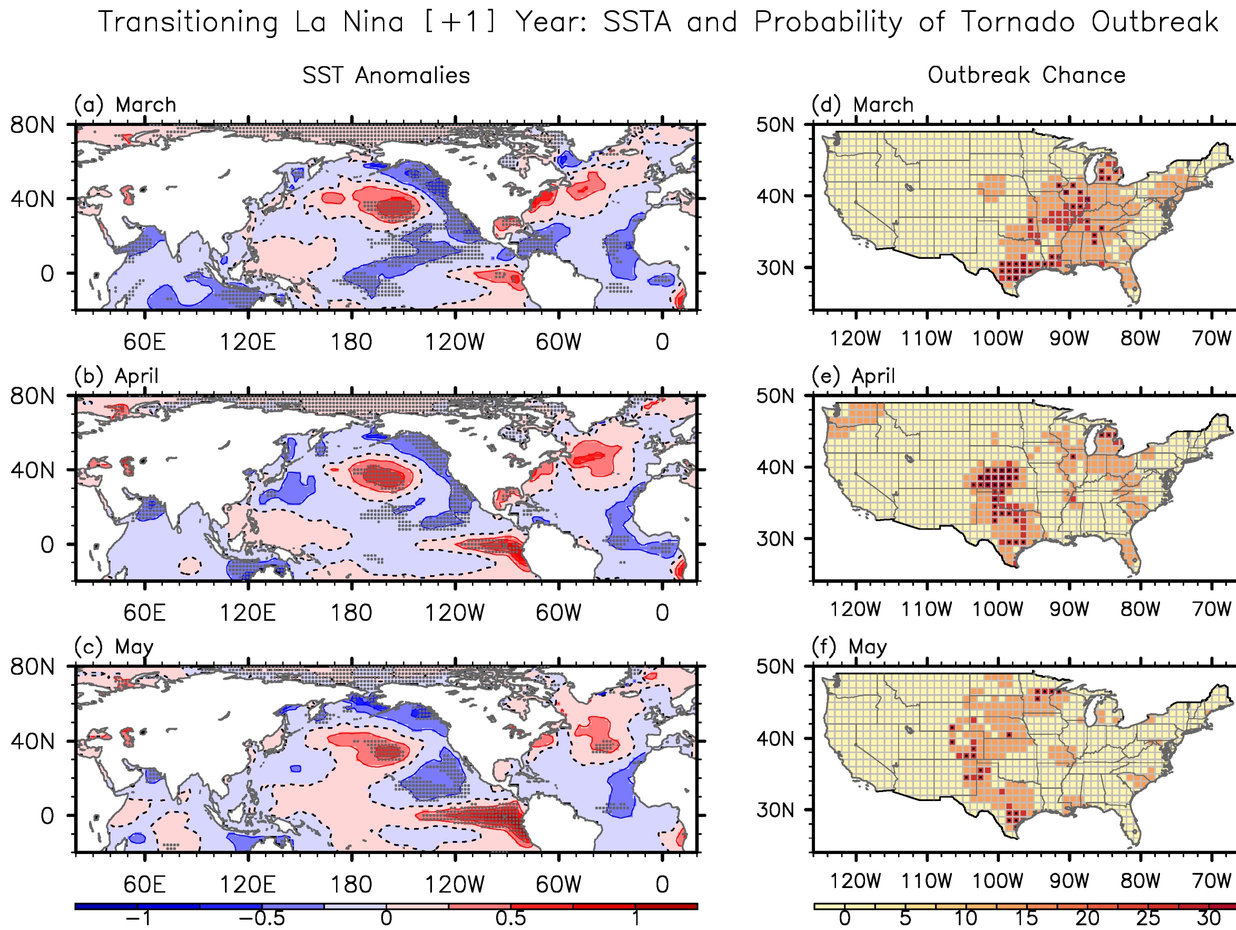

Figure S6. Composite (a-c) SSTAs for the transitioning El Niño case and (d-f) the corresponding probability of U.S. regional tornado outbreaks in (top row) March (+1), (middle row) April (+1) and (bottom row) May (+1). The gray dots in panels a-c indicate that the SSTAs are statistically significant at 90% based on a Student's *t*-test. The black dots in panels d-f indicate that the probability of tornado outbreaks is statistically significant at 90% based on a binomial test. The unit is in °C for the SSTAs and in % for the probability of tornado outbreaks.

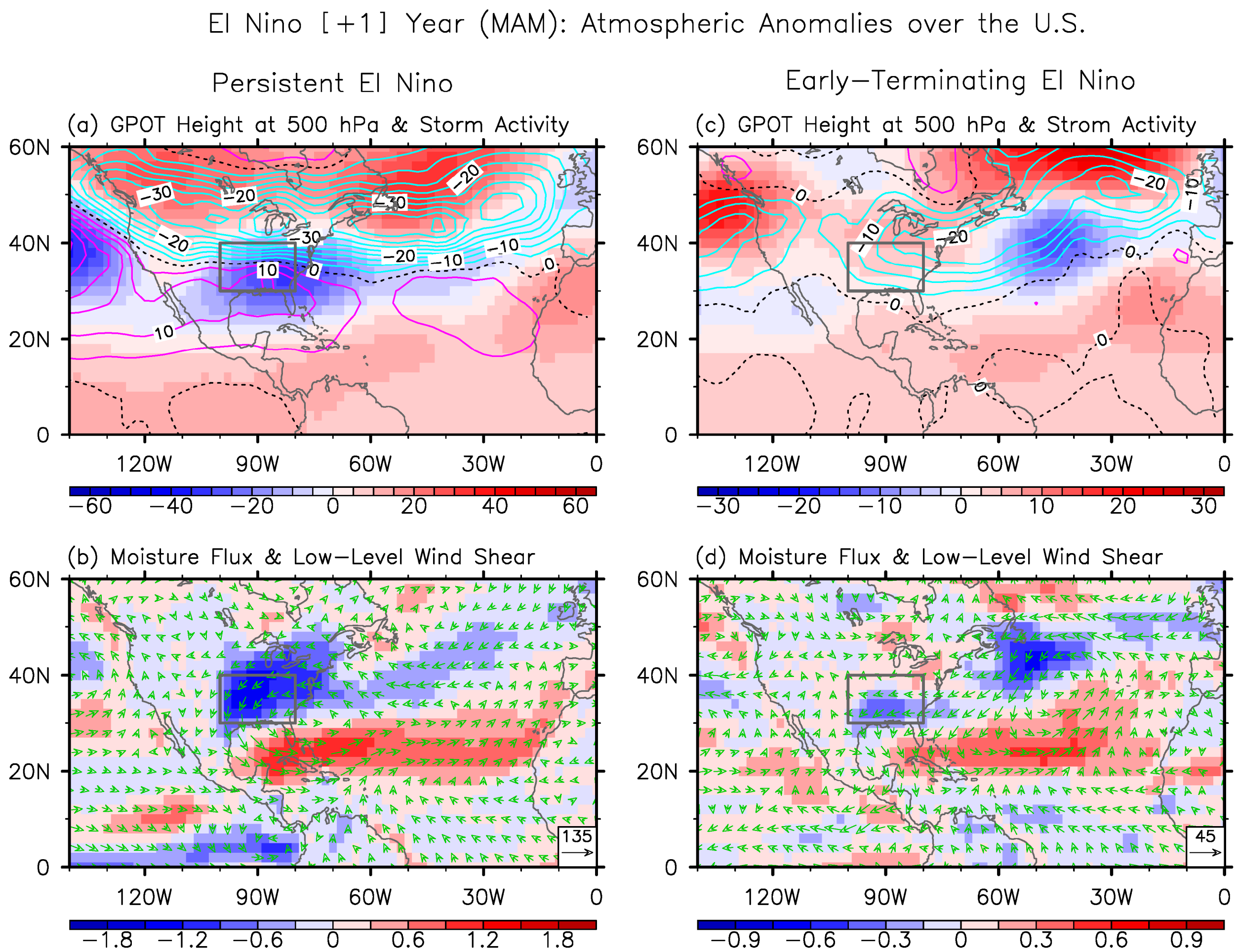

Figure S7. (upper row) Anomalous geopotential height at 500 hPa (color shades) and variance of 5day high-pass filtered meridional winds at 300 hPa (contours), and (lower row) anomalous moisture transport (vectors) and low-level vertical wind shear (850 - 1000 hPa; color shades) in MAM (+1) for (a,b) the persistent El Niño and (c,d) early-terminating El Niño cases. The units are in gpm for geopotential height, in m^2 s^{-2} for variance of meridional winds, in kg m^{-1} s^{-1} for moisture transport, and in m s^{-1} for vertical wind shear.

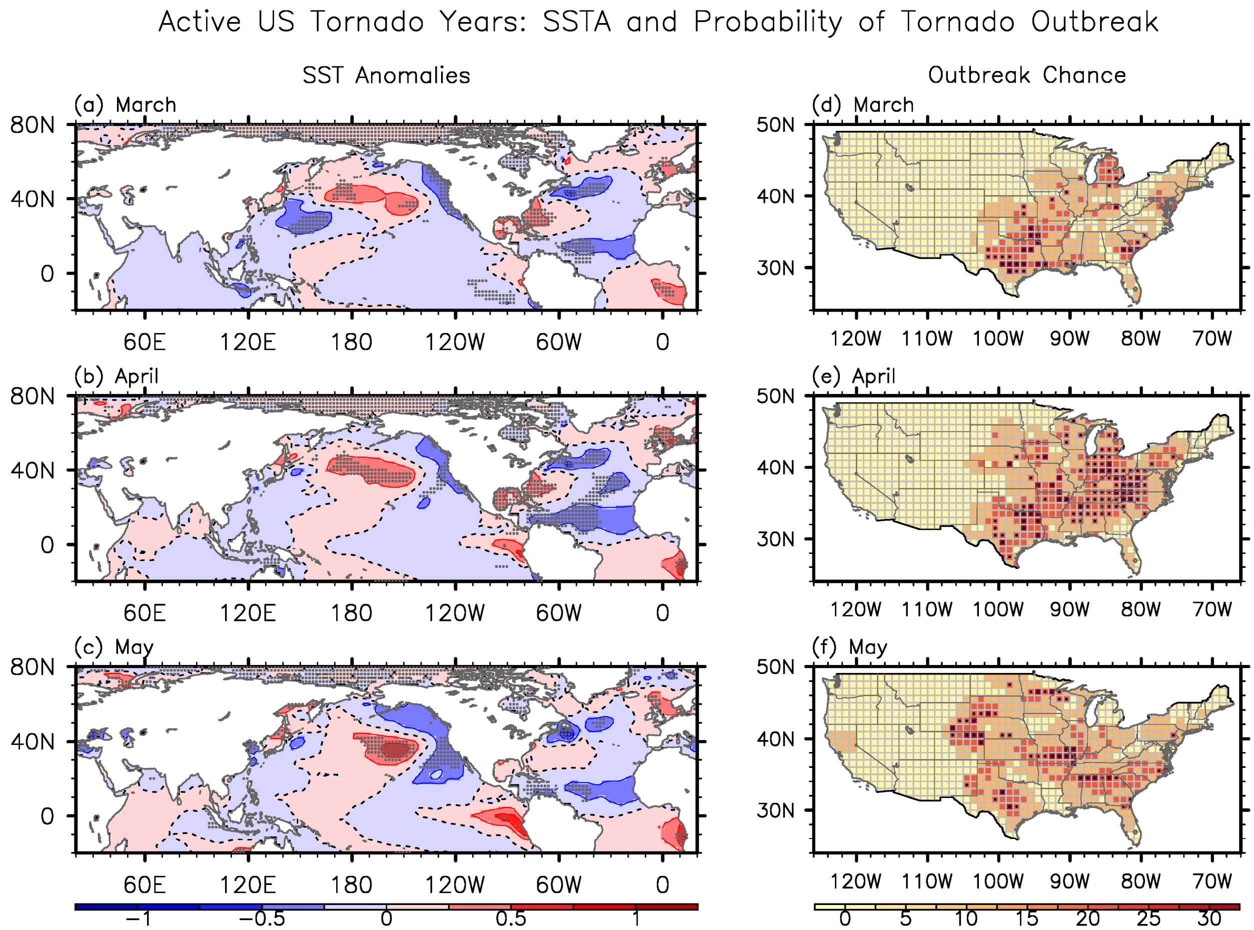

Figure S8. Composite (a-c) SSTAs for the 10 most active U.S. tornado years and (d-f) the corresponding probability of U.S. regional tornado outbreaks in (top row) March, (middle row) April and (bottom row) May. The gray dots in panels a-c indicate that the SSTAs are statistically significant at 90% based on a student-*t* test. The black dots in panels d-f indicate that the probability of tornado outbreaks is statistically significant at 90% based on a Chi-square test. The unit is in °C for the SSTAs and in % for the probability of tornado outbreaks.

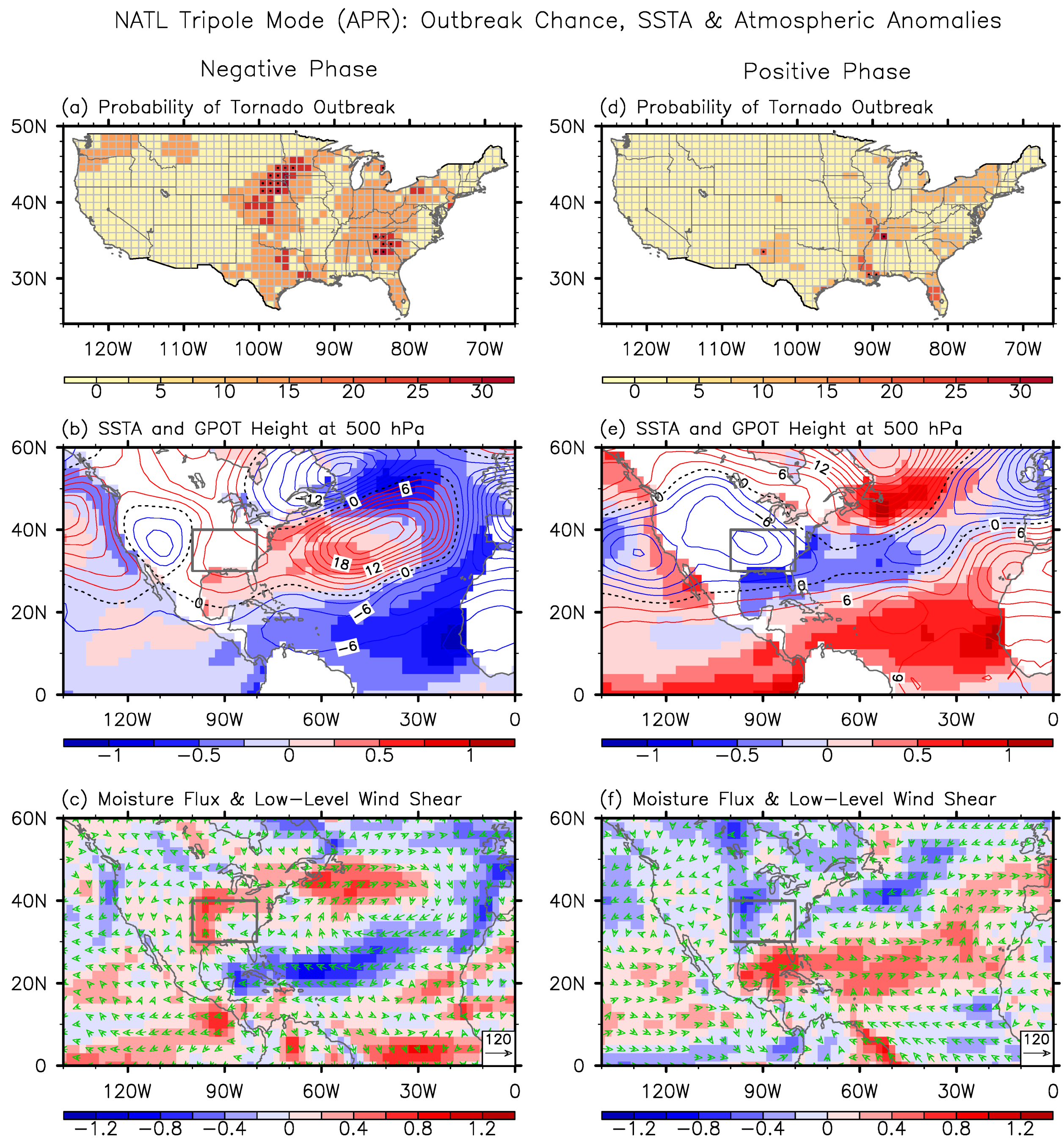

Figure S9. (top row) Probability of U.S. regional tornado, (middle row) composite SSTAs (color shades) and geopotential height anomalies at 500 hPa (contours), and (bottom row) low-level vertical wind shear anomalies (color shades) and moisture transport anomalies (vectors) in April for (a-c) the negative and (d-f) positive North Atlantic SST tripole. The unit is in % for the probability of tornado outbreaks, in °C for the SSTAs, in gpm for geopotential height, in kg m^{-1} s^{-1} for moisture transport, and in m s^{-1} for vertical wind shear.